

Second harmonic electromagnetic emission via Langmuir wave coalescence

A. J. Willes, P. A. Robinson, and D. B. Melrose

Department of Theoretical Physics and Research Center for Theoretical Astrophysics, School of Physics, University of Sydney, NSW 2006, Australia

(Received 25 May 1995; accepted 31 August 1995)

The coalescence of Langmuir waves to produce electromagnetic waves at twice the plasma frequency is considered. A simplified expression for the rate of production of second harmonic electromagnetic waves is obtained for a broad class of Langmuir spectra. In addition, two different analytic approximations are considered. The validity of the commonly used head-on approximation is explored, in which the two coalescing Langmuir waves are assumed to approach from opposite directions. This approximation breaks down at low Langmuir wavenumbers, and for narrow Langmuir wave spectra. A second, more general, approximation is introduced, called the narrow-spectrum approximation, which requires narrow spectral widths of the Langmuir spectra. The advantages of this approximation are that it does not break down at low Langmuir wavenumbers, and that it remains valid for relatively broad Langmuir wave spectra. Finally, the applicability of these approximations in treating harmonic radiation in type III solar radio bursts is discussed. © 1996 American Institute of Physics. [S1070-664X(96)02212-1]

I. INTRODUCTION

Second harmonic plasma emission occurs through the coalescence of two Langmuir waves, denoted here by $L+L' \rightarrow T$, where L and L' denote the two Langmuir waves and T denotes the (second harmonic) transverse wave. In most previous work on this process¹⁻⁴ it is assumed that the wavenumbers, k_L and $k_{L'}$, of the coalescing Langmuir waves far exceed that of the resulting transverse wave, k_T . This is known as the head-on approximation (HOA), because the coalescing Langmuir waves have $\mathbf{k}_{L'} \approx -\mathbf{k}_L$. For second harmonic plasma emission to proceed, in this approximation, a spectrum of Langmuir waves with roughly opposite wavenumbers is required. In solar type III bursts, for example, the primary Langmuir wave spectrum is produced by an unstable electron beam in the plasma. The secondary Langmuir spectrum, with wavevectors roughly antiparallel to those in the primary spectrum, is then widely accepted to be produced via another three-wave process: electrostatic backscatter decay. This process involves the decay $L \rightarrow L' + S$ of the primary Langmuir waves L into product Langmuir waves L' and ion-sound waves S . The kinematic constraints of conservation of energy and momentum imply that the backscattered Langmuir waves lie at wavenumbers $k_{L'} \approx k_0 - k_L$, with the offset k_0 (usually $\ll k_L$) dependent on the ion sound speed.³⁻⁵ Repeated backscatter decays are also possible,^{6,7} and a cascade of backscatter decays can produce a condensate of Langmuir waves at low wavenumbers. The number of such repeated backscatter decays is limited by kinematic constraints.⁸

The theory of nonlinear three-wave processes to explain fundamental and second harmonic emission in solar type III radio bursts was first proposed by Ginzburg and Zheleznyakov⁹ and later extended by Melrose.^{2,10,11} Further applications include type II solar radio bursts¹² and second harmonic emission upstream of the Earth's bowshock.¹³⁻¹⁵ An alternative mechanism to produce fundamental and harmonic

emission has recently appeared in the literature.¹⁶ This mechanism relies on the coexistence of high levels of Langmuir waves with a strong, unstable electron beam, whereas simulations and theory^{17,18} imply that the Langmuir waves coexist with an electron distribution that is plateaued by quasilinear relaxation. In addition, the high efficiency of this mechanism (for an unrelaxed beam) would imply that type III beams could not propagate to the observed large distances from the Sun because they would rapidly lose all their free energy to waves.¹⁸ Significantly, stochastic growth theory which assumes a relaxed marginally stable distribution as its starting point is able to account for most of the observations of type III Langmuir, ion sound and electromagnetic waves.^{19,5,20}

A relatively simple analytic expression for the emission rate of second harmonic waves, can be derived assuming the head-on approximation.^{3,4} Melrose and Stenhouse²¹ tested the validity of the HOA for isotropic power law Langmuir spectra, and found that it overestimates the emission rate at low wavenumbers, and for narrow spectra. Using the HOA, an expression for the degree of polarization of the harmonic radiation can also be derived.²² However, recent observations of the degree of polarization of harmonic emission in coronal type III solar radio bursts²³ are much higher than implied by theory, leading one to suspect the validity of the HOA in this case. We are thus motivated to find the bounds of validity of the HOA and to find a better approximation. Here, we concentrate on the emission rate of harmonic waves; we propose to discuss the polarization in a later paper.

In this paper, we model the primary and backscattered Langmuir spectra and evaluate an exact expression for the rate of production of second harmonic waves. The exact emission rate is expressed as a one-dimensional integral, and is evaluated numerically. An analytic expression for the emission rate is obtained with the HOA and is compared with the exact emission rate. We then introduce a more general *narrow-spectrum approximation* (NSA), for which an

analytic expression for the emission rate is also obtained. The NSA does not require $k_L, k_{L'} \gg k_T$, and thus is a better approximation at small Langmuir wavenumbers.

This paper is organized as follows. In Sec. II, an outline of the derivation of the exact emission rate is given. In Sec. III, the HOA emission rate is derived and compared to the exact emission rate. In Sec. IV, the NSA emission rate is derived and compared to the exact emission rate. In Sec. V, we consider the applicability of the head-on and narrow-spectrum approximations to type III solar radio bursts.

II. EMISSION RATE OF SECOND HARMONIC WAVES

In this section, we evaluate an integral expression for the rate of production of second harmonic waves. We consider a Langmuir wave spectrum with two components: the “forward” spectrum (e.g., beam-generated Langmuir waves), and the “backward” spectrum of Langmuir waves (e.g., back-scattered Langmuir waves). The emission rate, originally expressed as a multiple integral over the wavevectors of the two coalescing Langmuir waves, is reduced to a one-dimensional integral, which is in a suitable form to be approximated in a systematic way or it can be evaluated numerically.

The emission rate of transverse waves for the process $L(\omega_L(\mathbf{k}_1), \mathbf{k}_1) + L'(\omega_L(\mathbf{k}_2), \mathbf{k}_2) \rightarrow T(\omega_T(\mathbf{k}_T), \mathbf{k}_T)$ is given by the relation²¹

$$\frac{\partial T^T(\mathbf{k}_T)}{\partial t} = \frac{2}{\hbar \omega_p} \int \frac{d^3 \mathbf{k}_1}{(2\pi)^3} \int \frac{d^3 \mathbf{k}_2}{(2\pi)^3} u_{T12}(\mathbf{k}_T, \mathbf{k}_1, \mathbf{k}_2) \times T^L(\mathbf{k}_1) T^L(\mathbf{k}_2), \quad (1)$$

with

$$u_{T12}(\mathbf{k}_T, \mathbf{k}_1, \mathbf{k}_2) = \frac{(2\pi)^4 e^2 \hbar (k_1^2 - k_2^2)^2 |\hat{\mathbf{k}}_1 \times \hat{\mathbf{k}}_2|^2}{32 \epsilon_0 m_e^2 \omega_p k_T^2} \times \delta^3(\mathbf{k}_T - \mathbf{k}_1 - \mathbf{k}_2) \delta(\omega_T(\mathbf{k}_T) - \omega_L(\mathbf{k}_1) - \omega_L(\mathbf{k}_2)).$$

The transverse waves are described in terms of their effective temperature $T^T(\mathbf{k}_T)$ and the Langmuir waves (denoted by subscripts 1 and 2) in terms of their effective temperature $T^L(\mathbf{k}_{1,2})$, and $\hat{\mathbf{k}} = \mathbf{k}/k$. The delta function over frequency expresses conservation of energy, and that over wave vectors expresses conservation of momentum.

A. Functional form of Langmuir spectra

We consider a Langmuir spectrum with both forward and backward components. The distribution of Langmuir waves is assumed to be axially symmetric, with θ the angle between \mathbf{k} and the axis of symmetry. The Langmuir spectrum has the following form,

$$T^L(k, \theta) = T_f^L(k, \theta) + T_b^L(k, \theta),$$

$$T_f^L(k, \theta) = \xi T_f \exp \left[\frac{a(k) + b(k) \cos \theta}{K_f^2} \right],$$

$$T_b^L(k, \theta) = (1 - \xi) T_b \exp \left[\frac{c(k) + d(k) \cos \theta}{K_b^2} \right]. \quad (2)$$

The first term corresponds to the forward spectrum (subscript f), and the second term to the backward spectrum (subscript b). The functions $a(k)$, $b(k)$, $c(k)$ and $d(k)$ are arbitrary functions of k . Without loss of generality, we assume that \mathbf{k}_T lies in the $k_x - k_z$ plane. K_f is the characteristic width of the forward spectrum, K_b is the characteristic width of the backward spectrum, and $0 \leq \xi \leq 1$ is the fractional energy in the forward spectrum. The spectrum (2) has the normalization

$$\int \frac{d^3 \mathbf{k}}{(2\pi)^3} T^L(\mathbf{k}) = U, \quad (3)$$

where U is the energy density in the Langmuir waves. Typically, a wave from the forward spectrum coalesces with a Langmuir wave from the backward spectrum. It is also possible for two Langmuir waves from the same spectrum to coalesce, provided that $k_L, k_{L'} \leq k_T$.

In this paper we consider two types of Langmuir spectra, hereafter referred to as Gaussian and arc spectra. The *Gaussian spectrum* has a Gaussian profile, and peaks at wavenumber k_f along the beam (parallel) direction, and k_b in the opposite direction. For this case, the functions in the spectrum (2) are identified as

$$\begin{aligned} a(k) &= -k^2 - k_f^2, \\ b(k) &= 2k_f k, \\ c(k) &= -k^2 - k_b^2, \\ d(k) &= 2k_b k. \end{aligned} \quad (4)$$

The Gaussian Langmuir spectrum thus has the form

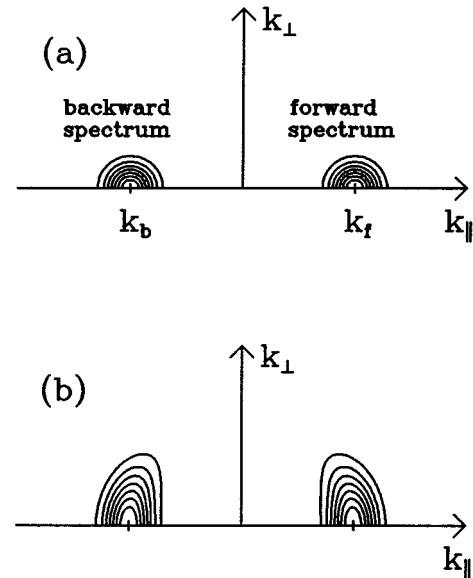


FIG. 1. (a) Gaussian and (b) arc Langmuir spectrum in wavenumber ($k_{\parallel} - k_{\perp}$) space. Each spectrum consists of two axially symmetric components; consisting of forward-propagating and backward-propagating waves, respectively. The spectral parameters are $k_f = (-)k_b = 5k_{T0}$, $K_f = K_b = 0.2k_f$, $\alpha = \beta = 10$. k_{T0} is the wavenumber of the product second harmonic wave. In all figures, the plasma frequency has the value $\omega_p = 1.5 \times 10^5 \text{ s}^{-1}$ and the thermal electron velocity $V_e = 1.5 \times 10^6 \text{ ms}^{-1}$, and the fraction of energy in the forward spectrum $\xi = 0.5$.

$$T^L(\mathbf{k}) = \xi T_f \exp\left[\frac{-(k_{\parallel} - k_f)^2 - k_{\perp}^2}{K_f^2}\right] + (1 - \xi) T_b \exp\left[\frac{-(k_{\parallel} - k_b)^2 - k_{\perp}^2}{K_b^2}\right], \quad (5)$$

where $k_{\parallel} = k \cos \theta$, $k_{\perp} = k \sin \theta$, and $T_f = 8 \pi^{3/2} U / K_f^3$, $T_b = 8 \pi^{3/2} U / K_b^3$. A typical Gaussian Langmuir spectrum is shown in Figure 1(a). An isotropic Gaussian spectrum is a special case, with $k_f = 0$ and $T_b = 0$.

The *arc spectrum* differs from the Gaussian spectrum in that it has a broader spread in perpendicular wavenumbers. The arc spectra more closely represent the functional form of the Langmuir spectra obtained through numerical solutions of the Zakharov equations, treating the process of backscatter decay.^{7,6}

The arc spectrum peaks at $k_z = k_f$ and $k_z = -k_b$ (with $k_f, k_b > 0$). In this case, the functions in the spectrum (2) are identified as

$$\begin{aligned} a(k) &= -k^2 + 2k_f k - k_f^2, \\ b(k) &= \alpha K_f^2, \\ c(k) &= -k^2 + 2k_b k - k_b^2, \\ d(k) &= -\beta K_b^2. \end{aligned} \quad (6)$$

The arc spectrum thus has the form

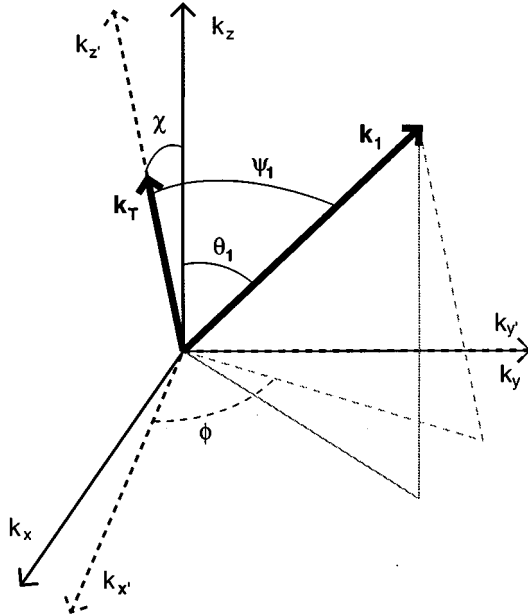


FIG. 2. Rotation of the coordinate axes about the k_y axis so that the $k_{z'}$ axis is parallel to \mathbf{k}_T .

$$T^L(k, \theta) = \xi T_f \exp\left[\frac{-(k - k_f)^2}{K_f^2}\right] \exp[\alpha \cos \theta], + (1 - \xi) T_b \exp\left[\frac{-(k - k_b)^2}{K_b^2}\right] \times \exp[-\beta \cos \theta]. \quad (7)$$

The angular extent of the arc spectra decreases with increasing α and β , with characteristic angular range $\cos^{-1}[(\alpha - 1)/\alpha]$. The parameter T_f satisfies

$$T_f = 2 \pi^2 \alpha U [\sinh \alpha \{3 k_f K^2 \exp(-k_f^2/K^2)/2 + \sqrt{\pi} K (K^2 + 2k_f^2) (1 + \operatorname{erf}(k_f/K))/4\}]^{-1}, \quad (8)$$

with a similar form for T_b . A typical arc Langmuir spectrum is shown in Figure 1(b).

B. Derivation of emission rate

Using the functional form of the Langmuir spectrum (2), the product of $T^L(k_1, \theta_1) T^L(k_2, \theta_2)$ in (1) gives four terms,

$$\begin{aligned} T^L(k_1, \theta_1) T^L(k_2, \theta_2) &= T_f^L(k_1, \theta_1) T_f^L(k_2, \theta_2) + T_f^L(k_1, \theta_1) T_b^L(k_2, \theta_2) \\ &+ T_b^L(k_1, \theta_1) T_f^L(k_2, \theta_2) + T_b^L(k_1, \theta_1) T_b^L(k_2, \theta_2). \end{aligned} \quad (9)$$

The four terms in (9) will be denoted by the subscripts ff, fb, bf and bb respectively (f for forward, b for backward). The following outline of the derivation considers only the fb term. The other three terms follow by analogy. The integral to be evaluated is of the form

$$\begin{aligned} \left[\frac{\partial T^T(\mathbf{k}_T)}{\partial t}\right]_{fb} &= \frac{e^2 \xi (1 - \xi) T_f T_b}{64 \pi^2 \epsilon_0 m_e^2 \omega_p^2} \int d^3 \mathbf{k}_1 \int d^3 \mathbf{k}_2 \\ &\times \frac{(k_1^2 - k_2^2)^2 |\hat{\mathbf{k}}_1 \times \hat{\mathbf{k}}_2|^2}{k_T^2} \\ &\times \exp\left[\frac{a(k_1) + b(k_1) \cos \theta_1}{K_f^2} + \frac{c(k_2) + d(k_2) \cos \theta_2}{K_b^2}\right] \delta^3(\mathbf{k}_T - \mathbf{k}_1 - \mathbf{k}_2) \\ &\times \delta(\omega_T(\mathbf{k}_T) - \omega_L(\mathbf{k}_1) - \omega_L(\mathbf{k}_2)). \end{aligned} \quad (10)$$

The integral over $d^3 \mathbf{k}_2$ is evaluated first. Using the delta function over wavevectors, the following substitutions are made in (10),

$$\mathbf{k}_2 = \mathbf{k}_T - \mathbf{k}_1, \quad k_2^2 = k_1^2 + k_T^2 - 2k_1 k_T \cos \psi, \quad (11)$$

with $\cos \psi = \hat{\mathbf{k}}_1 \cdot \hat{\mathbf{k}}_T$, and

$$\cos \theta_2 = \frac{k_T \cos \chi - k_1 \cos \theta_1}{\sqrt{k_1^2 + k_T^2 - 2k_1 k_T \cos \psi}}, \quad (12)$$

with $\cos \chi = \hat{\mathbf{k}}_T \cdot \hat{\mathbf{k}}_z$. Using these transformations, we find

$$\frac{(k_1^2 - k_2^2)^2}{k_T^2} = (2k_1 \cos \psi - k_T)^2, \quad (13)$$

$$|\hat{\mathbf{k}}_1 \times \hat{\mathbf{k}}_2|^2 = \frac{k_T^2 |\hat{\mathbf{k}}_1 \times \hat{\mathbf{k}}_T|^2}{k_2^2} = \frac{k_T^2 \sin^2 \psi}{k_1^2 + k_T^2 - 2k_1 k_T \cos \psi}. \quad (14)$$

The integral over $d^3 \mathbf{k}_1$ which remains is evaluated in a rotated coordinate frame in which the k_z axis is parallel to \mathbf{k}_T ($\hat{\mathbf{k}}_z$ is rotated in the $k_x - k_z$ plane). This coordinate transformation is illustrated in Fig. 2. The spherical polar coordinates are (k_1, ψ, ϕ) in the rotated frame. The polar angle θ_1 in the old frame is re-expressed as

$$\cos \theta_1 = \cos \chi \cos \psi - \sin \chi \sin \psi \cos \phi. \quad (15)$$

The integral (10) is then reduced to,

$$\begin{aligned} \left[\frac{\partial T^T(\mathbf{k}_T)}{\partial t} \right]_{\text{fb}} &= \frac{e^2 \xi (1 - \xi) T_f T_b}{64 \pi^2 \epsilon_0 m_e^2 \omega_p^2} \int_0^\infty dk_1 \int_{-1}^1 d \cos \psi \int_{-\pi}^\pi d \phi \frac{(2k_1 \cos \psi - k_T)^2 k_1^2 k_T^2 \sin^2 \psi}{k_2^2} \\ &\times \exp \left[\frac{a(k_1) + b(k_1) \cos \chi \cos \psi}{K_f^2} + \frac{k_2 c(k_2) + d(k_2)(k_T \cos \chi - k_1 \cos \chi \cos \psi)}{k_2 K_b^2} \right. \\ &\left. + \left(\frac{-b(k_1) \sin \chi \sin \psi}{K_f^2} + \frac{k_1 d(k_2) \sin \chi \sin \psi}{k_2 K_b^2} \right) \cos \phi \right] \delta(\omega_T(\mathbf{k}_T) - \omega_L(\mathbf{k}_1) - \omega_L(\mathbf{k}_2)), \end{aligned} \quad (16)$$

where $k_2(k_1) = \sqrt{k_1^2 + k_T^2 - 2k_1 k_T \cos \psi}$.

The integral over ϕ in (16) is evaluated using the relation,²⁴

$$I_0(z) = \frac{1}{2\pi} \int_{-\pi}^\pi d\phi e^{\pm z \cos \phi}, \quad (17)$$

where $I_0(z)$ is a zeroth order I-type Bessel function. The integral over k_1 is evaluated using the remaining delta function over frequencies and the dispersion relations for the Langmuir and transverse waves,

$$\omega_L(\mathbf{k}_L) \approx \omega_p \left(1 + \frac{3k_L^2}{2k_D^2} \right), \quad (18)$$

$$\omega_T(\mathbf{k}_T) = (\omega_p^2 + k_T^2 c^2)^{\frac{1}{2}}, \quad (19)$$

where $k_D = \omega_p / V_e$ is the Debye wavenumber, and V_e is the thermal electron speed. Hence,

$$\begin{aligned} &\delta(\omega_T(\mathbf{k}_T) - \omega_L(\mathbf{k}_1) - \omega_L(\mathbf{k}_T - \mathbf{k}_1)) \\ &= \delta \left(\omega_T - 2\omega_p - \frac{3V_e^2(2k_1^2 + k_T^2 - 2k_1 k_T \cos \psi)}{2\omega_p} \right) \\ &= \frac{\omega_p}{3V_e^2} \delta((k_1 - k_+)(k_1 - k_-)), \end{aligned}$$

with

$$k_+ = \frac{1}{2}(k_T \cos \psi + \sqrt{k_T^2 \cos^2 \psi + k_*^2 - 2k_T^2}), \quad (20)$$

$$k_- = \frac{1}{2}(k_T \cos \psi - \sqrt{k_T^2 \cos^2 \psi + k_*^2 - 2k_T^2}), \quad (21)$$

$$k_*^2 = \frac{4\omega_p(\omega_T(k_T) - 2\omega_p)}{3V_e^2} = 4k_1^2 + 2k_T^2 - 4k_1 k_T x. \quad (22)$$

Now, if we assume $V_e \leq c/4$, a valid assumption for most applications, then $k_- < 0$, and the integral over k_1 can be evaluated using the relation

$$\int_0^\infty dk_1 g(k_1) \delta((k_1 - k_+)(k_1 - k_-)) = \frac{g(k_+)}{k_+ - k_-}. \quad (23)$$

Hence (16) is reduced to the one-dimensional integral,

$$\begin{aligned} \left[\frac{\partial T^T(k_T, \chi)}{\partial t} \right]_{\text{fb}} &= \frac{e^2 \xi (1 - \xi) T_f T_b}{96 \pi \epsilon_0 \omega_p m_e^2 V_e^2} \int_{-1}^1 d \cos \psi \frac{k_1^2 (2k_1^2 - k_*^2 / 2)^2 \sin^2 \psi}{k_2^2 \sqrt{k_T^2 \cos^2 \psi + k_*^2 - 2k_T^2}} \times \exp \left[\frac{a(k_1) + b(k_1) \cos \chi \cos \psi}{K_f^2} \right. \\ &\left. + \frac{k_2 c(k_2) + d(k_2)(k_T \cos \chi - k_1 \cos \chi \cos \psi)}{k_2 K_b^2} \right] I_0 \left[\frac{b(k_1) \sin \chi \sin \psi}{K_f^2} - \frac{k_1 d(k_2) \sin \chi \sin \psi}{k_2 K_b^2} \right], \end{aligned} \quad (24)$$

with $k_1(\psi) = \frac{1}{2}(k_T \cos \psi + \sqrt{k_T^2 \cos^2 \psi + k_*^2 - 2k_T^2})$ and $k_2(k_1) = \sqrt{(k_*^2 - 2k_1^2)/2}$. This integral over ψ cannot be evaluated exactly analytically. It is the starting point for our numerical evaluation and analytic approximations in the following sections.

III. THE HEAD-ON APPROXIMATION

The HOA applies for $k_T \ll k_L, k_{L'}$. Wavevector conservation then implies that $\mathbf{k}_{L'} \approx -\mathbf{k}_L$; i.e., the Langmuir waves meet nearly head on. This is illustrated in Figure 3, with $\mathbf{k}_L + \mathbf{k}_{L'} = \mathbf{k}_T$. By making this assumption, an analytic ex-

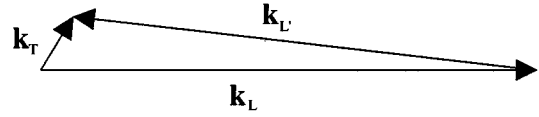


FIG. 3. Wavevector conservation for the coalescence process $L(\mathbf{k}_L) + L'(\mathbf{k}_{L'}) \rightarrow T(\mathbf{k}_T)$, where $\mathbf{k}_L + \mathbf{k}_{L'} = \mathbf{k}_T$. The condition for the HOA $k_L \gg k_T$ implies $\mathbf{k}_L \approx -\mathbf{k}_{L'}$.

pression for the rate of production can be derived from (24). The first step is to neglect terms of order k_T^2 , so that $k_1(\psi) \approx (k_T \cos \psi + k_*)/2$ is substituted into (24). We then neglect terms linear in k_T , to find

$$\left[\frac{\partial T^T(k_T, \chi)}{\partial t} \right]_{\text{fb}}^{\text{HOA}} = \frac{e^2 \xi (1 - \xi) T_f T_b}{96 \pi \epsilon_0 \omega_p m_e^2 V_e^2} \int_{-1}^1 d \cos \psi k_* k_T^2 \sin^2 \psi \cos^2 \psi \times \exp \left[\frac{a(k_*/2) + b(k_*/2) \cos \chi \cos \psi}{K_f^2} + \frac{c(k_*/2) - d(k_*/2) \cos \chi \cos \psi}{K_b^2} \right] \times I_0 \left[\left(\frac{b(k_*/2)}{K_f^2} - \frac{d(k_*/2)}{K_b^2} \right) \sin \chi \sin \psi \right]. \quad (25)$$

Only the first term in a large argument expansion of the Bessel function is then retained, to give $I_0(z) \approx e^z / \sqrt{2\pi z}$, which requires

$$\left(\frac{b(k_*/2)}{K_f^2} - \frac{d(k_*/2)}{K_b^2} \right) \sin \chi \sin \psi \gg 1. \quad (26)$$

Inclusion of all four terms from (9) yields,

$$\left[\frac{\partial T^T(k_T, \chi)}{\partial t} \right]^{\text{HOA}} = \frac{e^2 k_* k_T^2}{96 \pi \epsilon_0 \omega_p m_e^2 V_e^2} \left\{ \frac{4}{15} \xi^2 T_f^2 \exp \left[\frac{2a(k_*/2)}{K_f^2} \right] + \frac{\xi(1-\xi) T_f T_b}{\sqrt{2\pi \sin \chi (b(k_*/2)/K_f^2 - d(k_*/2)/K_b^2)}} \times \int_{-1}^1 d \cos \psi \sin^{3/2} \psi \cos^2 \psi \exp \left[\frac{a(k_*/2)}{K_f^2} + \frac{c(k_*/2)}{K_b^2} + \left(\frac{b(k_*/2)}{K_f^2} - \frac{d(k_*/2)}{K_b^2} \right) \cos(\psi - \chi) \right] + \frac{\xi(1-\xi) T_f T_b}{\sqrt{2\pi \sin \chi (b(k_*/2)/K_f^2 - d(k_*/2)/K_b^2)}} \int_{-1}^1 d \cos \psi \sin^{3/2} \psi \cos^2 \psi \exp \left[\frac{a(k_*/2)}{K_f^2} + \frac{c(k_*/2)}{K_b^2} - \left(\frac{b(k_*/2)}{K_f^2} - \frac{d(k_*/2)}{K_b^2} \right) \cos(\psi + \chi) \right] + \frac{4}{15} (1 - \xi)^2 T_b^2 \exp \left[\frac{2c(k_*/2)}{K_b^2} \right] \right\}. \quad (27)$$

For $(b(k_*/2)/K_f^2 - d(k_*/2)/K_b^2) \gg 1$, as assumed for the large argument Bessel function expansion (26), the argument of the exponential in each of the two integrals in (27) strongly peaks at $\psi = \chi$ and $\psi = \pi - \chi$ respectively. We then integrate using the method of steepest descents, to give

$$\left[\frac{\partial T^T(k_T, \chi)}{\partial t} \right]^{\text{HOA}} = \frac{e^2 k_* k_T^2}{48 \pi \epsilon_0 \omega_p m_e^2 V_e^2} \left\{ \frac{4}{15} \left(\xi^2 T_f^2 \exp \left[\frac{2a(k_*/2)}{K_f^2} \right] + (1 - \xi)^2 T_b^2 \exp \left[\frac{2c(k_*/2)}{K_b^2} \right] \right) + \frac{\xi(1-\xi) T_f T_b \sin^2 \chi \cos^2 \chi}{(b(k_*/2)/K_f^2 - d(k_*/2)/K_b^2)} \exp \left[\frac{a(k_*/2) + b(k_*/2)}{K_f^2} + \frac{c(k_*/2) - d(k_*/2)}{K_b^2} \right] \right\}. \quad (28)$$

A. HOA for Gaussian spectra

From (4) and (28), the HOA emission rate for Gaussian Langmuir spectra is

$$\left[\frac{\partial T^T(k_T, \chi)}{\partial t} \right]^{\text{HOA}} = \frac{e^2 k_T^2}{96\pi\epsilon_0\omega_p m_e^2 V_e^2} \left\{ \frac{4}{15} \left(\xi^2 T_f^2 \exp\left[\frac{-(k_*^2 + 4k_f^2)}{2K_f^2} \right] + (1-\xi)^2 T_b^2 \exp\left[\frac{-(k_*^2 + 4k_b^2)}{2K_b^2} \right] \right) + \frac{\xi(1-\xi)T_f T_b \sin^2 \chi \cos^2 \chi}{(k_f/K_f^2 - k_b/K_b^2)} \exp\left[\frac{-(k_* - 2k_f)^2}{4K_f^2} + \frac{-(k_* - 2k_b)^2}{4K_b^2} \right] \right\}. \quad (29)$$

The value of k_T at which the emission rate peaks can be determined from frequency conservation, $\omega_T(\mathbf{k}_T) = \omega_L(\mathbf{k}_1) - \omega_L(\mathbf{k}_2)$, using the dispersion relations (18) and (19) and by assuming $k_1 = k_f$ and $k_2 = k_b$. This yields

$$k_{T\text{max}} = k_{T0}(1 + \Delta), \quad (30)$$

with $k_{T0} = \sqrt{3}\omega_p/c$, and $\Delta = (k_f^2 + k_b^2)/k_D^2 \ll 1$, where $k_D = \omega_p/V_e$. Two cases are considered here; where the primary and backscattered Langmuir spectra are symmetrically placed; i.e., $k_b = -k_f$, and where the backscattered spectrum is offset by k_0 , so that $k_b = k_0 - k_f$.

1. Symmetric spectra

Figure 4 shows contours of equal emission rate as a function of emission angle χ and k_T for symmetric Langmuir spectra (see Fig. 1) for (a) the exact emission rate (24) and (b) the HOA, where $k_f = -k_b = 5k_{T0}$, $K_f = K_b = 0.2k_f$. These parameters are in the regime where $k_f \gg k_T$. Here, the maximum HOA emission rate is 1.4 times greater than the exact

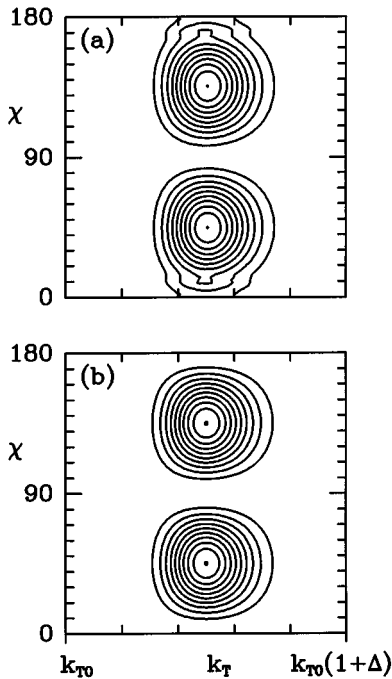


FIG. 4. Comparison of the emission rate as a function of emission angle χ and wavenumber k_T for symmetric Gaussian Langmuir spectra for (a) the exact emission rate and (b) the HOA, with $k_f = -k_b = 5k_{T0}$, $K_f = K_b = 0.2k_f$. The equally spaced contours (linear in the emission rate) range from zero to the maximum value.

value. The HOA emission rate always peaks at $\chi = 45^\circ, 135^\circ$ due to the $\sin^2 \chi \cos^2 \chi$ term in (28), which agrees well with the exact emission rate. The dependence of the emission rate on k_T and χ is similar for the exact and HOA emission rates. Hence it is valid to consider only the maximum emission rate when comparing the exact and HOA emission rates.

Figure 5 shows the maximum emission rate (maximized over χ and k_T) vs. k_f , for both the exact and HOA emission rates. The HOA drastically overestimates the exact emission rate at low Langmuir wavenumbers. Indeed, we find that the approximation worsens for narrower Langmuir spectra, where it becomes increasingly difficult to satisfy the kinematic constraints. At low wavenumbers, $k_f \approx \frac{1}{2}k_T$, there is an additional peak in the exact emission rate, due to two Langmuir waves that propagate in roughly the same direction coalescing to produce a transverse wave with wavenumber k_T , as seen in Fig. 6. The peak emission rate for this process occurs at $\chi = 0^\circ, 180^\circ$. The extended low-level contours near $\chi = 0^\circ$ and 180° in Fig. 4(a) are also due to this effect. The HOA does not reproduce this feature, as it assumes the two coalescing Langmuir waves are propagating in opposite directions.

2. Offset spectra

The offset Langmuir spectra, where the backward spectrum peaks at lower wavenumbers than the forward spectrum, is physically relevant because the process of backscatter decay produces backward propagating Langmuir waves with $|k_b| < k_f$. Figure 7 shows the contour plots of emission rate for offset backscattered spectra with $k_f = 5k_{T0}$, $k_b = 4.5k_{T0}$ and $K_f = K_b = 0.2k_f$ for (a) the exact emission rate, and (b) the HOA. Here, the offset is $k_0 = k_{T0}/2$. In this case,

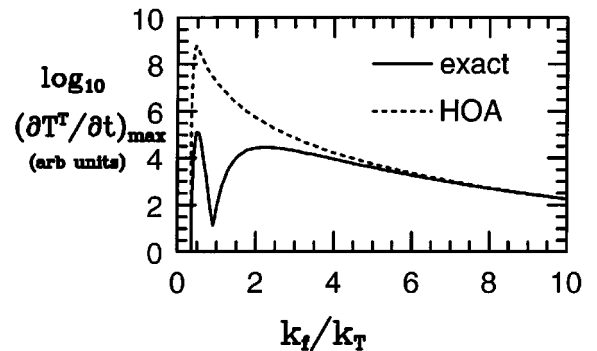


FIG. 5. Maximum emission rate (arbitrary units) of second harmonic transverse electromagnetic waves as a function of k_f , the peak wavenumber of the primary Gaussian Langmuir spectrum, with $k_b = -k_f$ and $K_f = K_b = 0.2k_f$. The exact emission rate is marked with a solid line, the HOA with a dashed line.

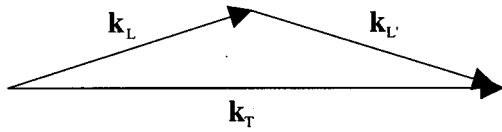


FIG. 6. Langmuir wave coalescence at low wavenumbers. Two Langmuir waves with wavenumbers $k_L, k_{L'} \approx \frac{1}{2}k_T$ coalesce to produce a transverse wave, with wavenumber k_T .

the maximum emission rate is comparable for the HOA and exact cases, because wavevector conservation is more easily satisfied for these asymmetric spectra than for symmetric spectra. Figure 7(a) displays a higher rate for $\chi < 90^\circ$ than for $\chi > 90^\circ$, corresponding to more transverse waves produced in the forward direction. Wavevector conservation, $\mathbf{k}_T = \mathbf{k}_L + \mathbf{k}_{L'}$, with on average k_L (forward waves) greater than $k_{L'}$ (backward waves), implies that \mathbf{k}_T is biased in the forward direction. The HOA [Fig. 7(b)] does not reproduce this asymmetry, but has equal peaks in emission rate for $\chi = 45^\circ$ and $\chi = 135^\circ$.

The accuracy of the HOA in predicting the maximum emission rate for offset Langmuir spectra depends on the magnitude of the offset k_0 . For $k_0 = 0$ (symmetric spectra), the HOA overestimates the exact emission rate (see Fig. 5). The HOA is most accurate for $k_0 \lesssim k_{T0}$, where the kinematic constraints are most easily satisfied; i.e., where the most Langmuir waves from the forward and backward spectra can coalesce to produce a transverse wave with wavenumber k_{T0} and $\chi = 45^\circ$. Figure 8 shows the maximum emission rate as a function of k_f , with $k_0 = k_{T0}/\sqrt{2}$. Comparing Fig. 8

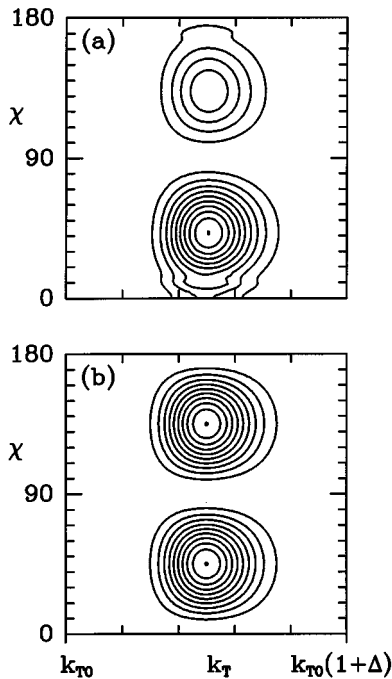


FIG. 7. Emission rate as a function of emission angle χ and wavenumber k_T for offset Gaussian Langmuir spectra for (a) the exact emission rate, and (b) the HOA, with $k_f = 5k_{T0}$, $k_b = 4.5k_{T0}$, $K_f = K_b = 0.2k_f$.

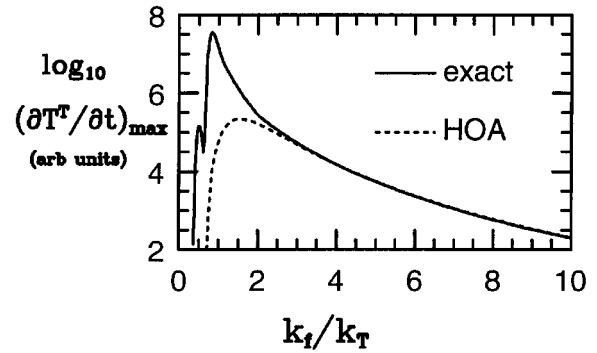


FIG. 8. Maximum emission rate (arbitrary units) as a function of k_f for offset backscattered Gaussian spectra ($k_0 \lesssim k_T$, $k_b = k_0 - k_f$, and $K_f = K_b = 0.2k_f$). The exact solution is marked with a solid line, the HOA with a dashed line.

with Fig. 5 ($k_0 = 0$) and Fig. 9 ($k_0 \gg k_{T0}$) illustrates this point. Again, the HOA breaks down at low k_L .

For larger offsets ($k_0 \gtrsim k_{T0}$), the HOA always underestimates the exact emission rate. Figure 9 shows the maximum emission rate as a function of k_f , for $k_0 = 2k_{T0}$. For wavenumbers $k_f \lesssim 2k_{T0}$, the backscattered spectrum also lies at positive wavenumbers, and the HOA emission rate, which assumes oppositely propagating Langmuir waves, is zero. The peaks at $k_f = 3k_{T0}/2$ and $k_f = 5k_{T0}/2$ correspond to $k_b = \pm k_{T0}/2$ and thus are similar to the peak at $k_f = k_{T0}/2$ in Fig. 5.

B. HOA for arc spectra

The HOA emission rate for arc spectra is similar in form to (29). Figure 10 shows emission rate contours for symmetric arc spectra (see Fig. 2), with $k_f = -k_b = 5k_{T0}$, $K_f = K_b = 0.2k_f$, $\alpha = \beta = 10$, for (a) the exact, and (b) the HOA emission rate. As for the symmetric Gaussian spectrum in Figure 4, the HOA overestimates the exact emission rate by a factor of 1.4; however, here the maximum emission rate occurs at lower angles $\chi \approx 20^\circ, 160^\circ$, due to the different spectral shape and broader spread in perpendicular wavenumbers in the arc spectrum. The peak at angles $\chi = 45^\circ, 135^\circ$ is still evident, but not as strong. As for the Gaussian spectra, the HOA predicts the maximum emission rate to

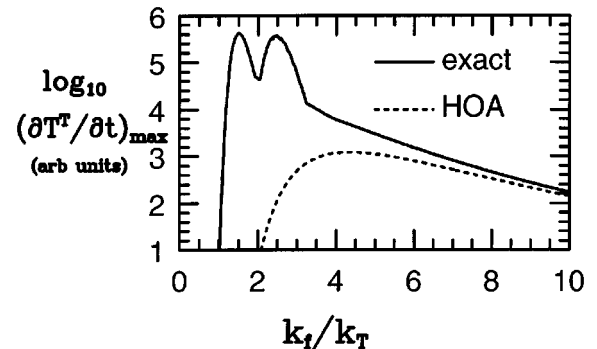


FIG. 9. Maximum emission rate (arbitrary units) as a function of k_f , with a larger offset of the backscattered spectrum. ($k_0 = 2k_T$, $k_b = k_0 - k_f$, and $K_f = K_b = 0.2k_f$). The exact solution is marked with a solid line, the HOA with a dashed line.

occur at angles $\chi=45^\circ, 135^\circ$, and the peaks are not as broad as for the exact emission rate. For the offset arc spectra, as for the symmetric spectra, there is little qualitative difference between the emission rate for the Gaussian spectra and the arc spectra.

IV. NARROW SPECTRUM APPROXIMATION

In the previous section, the HOA is shown to break down for $k_L \leq k_T$. In this section an alternative approximation is considered, where the assumption $k_T \leq k_L$, k_L' is not made, so as to better approximate the emission rate at low Langmuir wavenumbers. Instead, we make a narrow spec-

trum approximation (NSA), in which we assume $K_f/k_f \ll 1$ and $K_b/k_b \ll 1$. This allows the replacement of the Bessel function in (24) with the first term in its large argument expansion. This is valid for

$$\left(\frac{b(k_1)}{K_f^2} - \frac{k_1 d(k_2)}{k_2 K_b^2} \right) \sin \chi \sin \psi \gg 1, \quad (31)$$

which for both Gaussian and arc spectra is automatically satisfied for K_f/k_f , $K_b/k_b \ll 1$. As for the HOA, the integrand peaks strongly at $\psi = \chi$. We assume $\psi = \chi$ elsewhere in the integrand, and again integrate by steepest descents, to find

$$\left[\frac{\partial T^T(k_T, \chi)}{\partial t} \right]_{\text{fb}}^{\text{NSA}} = \frac{e^2 \xi (1 - \xi) T_f T_b k_1^2 (4k_1^2 - k_*^2)^2 \sin^2 \chi}{384 \pi \epsilon_0 \omega_p m_e^2 V_e^2 k_2^2 \sqrt{(k_T^2 \cos^2 \chi + k_*^2 - 2k_T^2)} (b(k_1)/K_f^2 - k_1 d(k_2)/(k_2 K_b^2))} \times \exp \left[\frac{a(k_1) + b(k_1)}{K_f^2} + \frac{c(k_2)}{K_b^2} + \frac{d(k_2)(k_T \cos \chi - k_1)}{k_2 K_b^2} \right], \quad (32)$$

with $k_1(k_T, \chi) = \frac{1}{2}(k_T \cos \chi + \sqrt{k_T^2 \cos^2 \chi + k_*^2 - 2k_T^2})$ and $k_2(k_1) = \sqrt{k_*^2/2 - k_1^2}$.

The NSA is more accurate in the range $0 \leq \chi \leq \pi/2$ than $\pi/2 \leq \chi \leq \pi$. This is because the peak at $\psi = \chi$ is sharper in the range $0 \leq \chi \leq \pi/2$ than for $\pi/2 \leq \chi \leq \pi$. This leads to the undesirable situation where, for symmetric Langmuir spectra (e.g., for Gaussian spectra, $k_b = -k_f$ and $K_b = K_f$), the NSA emission rate is asymmetric about $\chi = 90^\circ$, whereas the exact emission rate is symmetric about $\chi = 90^\circ$. The symmetry is regained by evaluating the emission rate in two regimes. For the range $0 \leq \chi \leq 90^\circ$, we use (32) as it stands. For the range $90^\circ \leq \chi \leq 180^\circ$, a change of variables is made so that (32) is evaluated in the range $0 \leq \chi \leq 90^\circ$. This is achieved by reflecting the forward and backward Langmuir spectra about $k_{\parallel} = 0$ and replacing χ by $\pi - \chi$ in (32). That is, we replace the forward spectrum with the backward spectrum and vice versa, so that the emission rate in the range $90^\circ < \chi < 180^\circ$ is

now evaluated in the range $0^\circ < \chi < 90^\circ$ where the NSA is more accurate. This method is also applied to offset spectra.

The bf term is obtained by making the replacements $a \rightarrow c, b \rightarrow d, c \rightarrow a$, and $d \rightarrow b$. The NSA is not valid for the ff and bb terms because it becomes increasingly difficult for two wavevectors from the same (either forward or backward) spectrum to add together to give \mathbf{k}_T in the limit as the width of the spectrum goes to zero. Due to the $\sin^2 \chi$ term in (32), the coalescing Langmuir waves cannot both be propagating in the parallel direction. Hence, as for the HOA, the NSA fails to reproduce the low wavenumber peak in emission rate due to the coalescence of two Langmuir waves propagating in the same direction.

A. NSA for Gaussian spectra

Using the forms for a, b, c and d in (4), and imposing the symmetry discussed above, (32) becomes

$$\left[\frac{\partial T^T(k_T, \chi)}{\partial t} \right]_{\text{fb}}^{\text{NSA}} = \frac{e^2 \xi (1 - \xi) T_f T_b k_1^2 (2k_1^2 - k_*^2/2)^2 \sin^2 \chi}{192 \pi \epsilon_0 \omega_p m_e^2 V_e^2 k_1 k_2^2 \sqrt{(k_T^2 \cos^2 \chi + k_*^2 - 2k_T^2)} (k_f/K_f^2 - k_b/K_b^2)}, \times \exp \left[\frac{-(k_1 - k_f)^2}{K_f^2} + \frac{-k_2^2 - k_b^2 + 2k_b(k_T \cos \chi - k_1)}{K_b^2} \right], \quad (33)$$

for $0 \leq \chi \leq \pi/2$, and

$$\left[\frac{\partial T^T(k_T, \chi)}{\partial t} \right]_{\text{fb}}^{\text{NSA}} = \frac{e^2 \xi (1 - \xi) T_f T_b k_1^2 (2k_1^2 - k_*^2/2)^2 \sin^2 \chi}{192 \pi \epsilon_0 \omega_p m_e^2 V_e^2 k_1 k_2^2 \sqrt{(k_T^2 \cos^2 \chi + k_*^2 - 2k_T^2)} (k_f/K_f^2 - k_b/K_b^2)} \times \exp \left[\frac{-(k_1 + k_b)^2}{K_b^2} + \frac{-k_2^2 - k_f^2 - 2k_f(-k_T \cos \chi - k_1)}{K_f^2} \right], \quad (34)$$

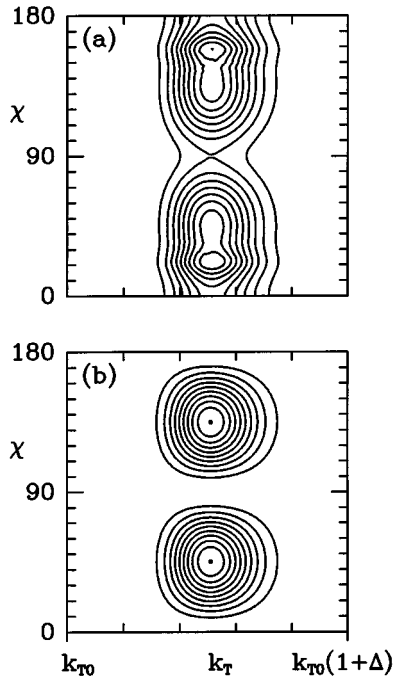


FIG. 10. Emission rate as a function of emission angle χ and wavenumber k_T for arc Langmuir spectra in Figure 2 for (a) the exact emission rate, and (b) the HOA, with $k_f = -k_b = 5k_{T0}$, $K_f = K_b = 0.2k_f$, $\alpha = \beta = 10$.

for $\pi/2 \leq \chi \leq \pi$. From (4) and (9), the bf term is obtained by making the replacements: $k_f \rightarrow k_b$, $K_f \rightarrow K_b$, $k_b \rightarrow k_f$ and $K_b \rightarrow K_f$ in (33) and (34).

1. Symmetric spectra

Figure 11 shows the NSA emission rate for the same parameters as Fig. 4 ($k_f = -k_b = 5k_{T0}$, $K_f = K_b = 0.2k_f$). In this case the maximum emission rate is 0.93 times the exact maximum emission rate, compared to a factor of 1.4 for the HOA. The dependence of the emission rate on k_T and χ is similar to the exact emission rate. Hence the maximum emission rate is an adequate point of comparison between the exact and NSA emission rates. Figure 12 shows the maximum emission rate as a function of k_f for both the exact and

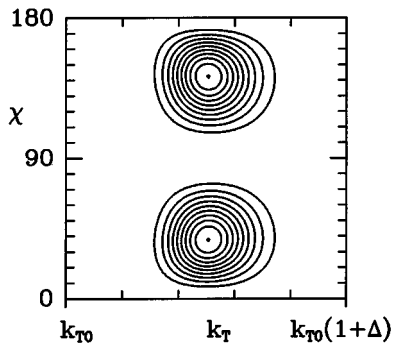


FIG. 11. Emission rate as a function of emission angle χ and wavenumber k_T for Gaussian Langmuir spectra in Figure 1, assuming the NSA $k_f = -k_b = 5k_{T0}$, $K_f = K_b = 0.2k_f$.

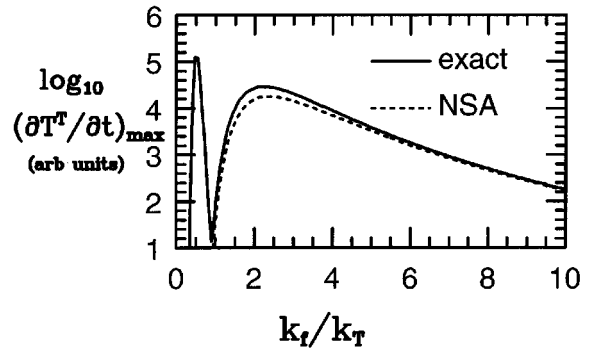


FIG. 12. Maximum emission rate (arbitrary units) as a function of k_f , with no offset (symmetric spectra). ($k_b = -k_f$, and $K_f = K_b = 0.2k_f$). The exact solution is marked with a solid line, the NSA with a dashed line.

the NSA emission rates. The agreement is excellent, down to $k_f \approx k_T$, but the NSA does not reproduce the peak at $k_f = k_{T0}/2$.

2. Offset spectra

Figure 13 shows the NSA emission rate for the same parameters as Fig. 7 ($k_f = 5k_{T0}$, $k_b = 4.5k_{T0}$, $K_f = K_b = 0.2k_f$). In this case the maximum NSA emission rate is 0.95 times the maximum exact emission rate. Unlike the HOA, the NSA displays the higher emission rate for $\chi < 90^\circ$ (see Fig. 7). Figure 14 shows the maximum emission rate as a function of k_f for both the exact emission rate and the NSA for the same parameters as Fig. 9 (offset $k_0 = 2k_T$), displaying excellent agreement for $k_f > 3k_{T0}$. For $k_f > 3k_{T0}$, the NSA still closely agrees with the fb and bf terms of the exact emission rate. The two peaks at $k_f = 3k_{T0}/2$ and $k_f = 5k_{T0}/2$ are due to the ff and bb terms, which the NSA cannot approximate. Nevertheless, in this regime, the NSA is preferable to the HOA, which underestimates the emission rate by many orders of magnitude.

In addition, the NSA works reasonably well for wider Langmuir spectra. For both symmetric and offset spectra, the NSA agrees with the exact emission rate to within an order of magnitude, for widths $K_f \leq 0.5k_f$. This is sufficient accuracy to calculate the emission rate for experimentally determined parameters of the Langmuir spectra, where the signifi-

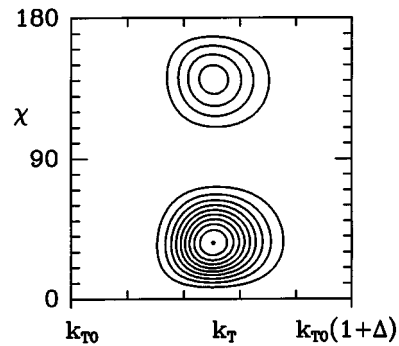


FIG. 13. Emission rate as a function of emission angle χ and wavenumber k_T for offset Gaussian Langmuir spectra, assuming the NSA $k_f = 5k_{T0}$, $k_b = 4.5k_{T0}$, $K_f = K_b = 0.2k_f$.

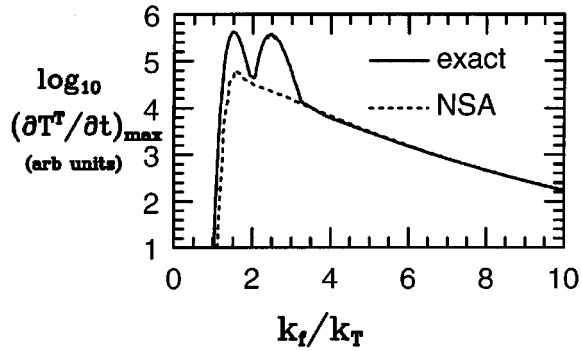


FIG. 14. Maximum emission rate (arbitrary units) as a function of k_f , with a large offset in the backscattered spectrum. ($k_0 = 2k_T$, $k_b = k_0 - k_f$, and $K_f = K_b = 0.2k_f$). The exact solution is marked with a solid line, the NSA with a dashed line.

cant uncertainties in the spectral parameters lead to even larger uncertainties in the emission rate because of the exponential form of the Langmuir spectra.

B. Arc spectra

The expression for the NSA emission rate is similar in form to that for the Gaussian spectra. For the arc spectra, there is little change to the conclusions made for the symmetric and offset Gaussian Langmuir spectra.

V. SOLAR TYPE III BURSTS

In this section, we discuss the applicability of the HOA and NSA to coronal and interplanetary type III bursts. The position and width of the Langmuir spectra for these bursts are determined from the observed electron beam speed and width. The wavenumber offset is determined from local plasma parameters. From this information the validity of the HOA and the NSA can be determined.

The accuracy of the HOA depends on two criteria. The first is $k_L \gg k_T$, the basic HOA assumption. The second criterion is that both the forward and backward Langmuir spectra must be sufficiently broad so as to allow wavevector conservation when a Langmuir wave from the forward spectrum coalesces with one from the backward spectrum to produce a transverse wave with wavenumber k_T . Larger widths are also required to compensate for large offsets. Hence, the spectral width must satisfy

$$K_L \geq |k_0 - k_T|. \quad (35)$$

The kinematic constraints are best satisfied for $k_0 \approx k_T$, where there is correspondingly less restriction on K_L .

The (forward) Langmuir wavenumber k_{beam} is related to the electron beam speed v_{beam} by $k_{\text{beam}} = \omega_p / v_{\text{beam}}$. The spectral width is related to the beam width by

$$\frac{K_{\text{beam}}}{k_{\text{beam}}} \approx \frac{\Delta v_{\text{beam}}}{v_{\text{beam}}}. \quad (36)$$

The backscatter offset k_0 is dependent on the ion sound speed v_s , with⁵

$$k_0 = \frac{2\omega_p v_s}{3V_e^2} \approx \frac{2}{3} \sqrt{\frac{\gamma m_e \omega_p}{m_i V_e}}, \quad (37)$$

where m_e and m_i are the electron and ion masses; $\gamma = 1 + 3T_i/T_e$ with T_e and T_i the electron and ion temperatures. We assume $\gamma = 1$ in the following discussion. Using the above two criteria, with a given observed beam speed v_{beam} and width $\Delta v_{\text{beam}}/v_{\text{beam}}$, the HOA is applicable provided that

$$v_{\text{beam}} \leq c/\sqrt{3}, \quad (38)$$

$$\frac{\Delta v_{\text{beam}}}{v_{\text{beam}}} \geq \left| \frac{2}{3V_e} \sqrt{\frac{\gamma m_e}{m_i}} - \frac{\sqrt{3}}{c} \right| v_{\text{beam}}. \quad (39)$$

A similar relation to (39) derived by Robinson and Cairns²⁰ did not include the absolute value sign, and hence covers too great a range. Typically, electron beam speeds are observed to be in the range $v_{\text{beam}} = (0.04 - 0.30)c$ for both coronal and interplanetary type III bursts,²⁵⁻²⁷ so that (38) is reasonably well satisfied, except for the fastest beams. Typical values of the thermal electron speed are $V_e = 5.0 \times 10^6 \text{ m s}^{-1}$ for coronal bursts and $V_e = 1.5 \times 10^6 \text{ m s}^{-1}$ for interplanetary bursts at 1 AU from the Sun. Hence, using (39), the coronal bursts require $\Delta v_{\text{beam}}/v_{\text{beam}} \geq 0.8v_{\text{beam}}/c$ and the interplanetary bursts require $\Delta v_{\text{beam}}/v_{\text{beam}} \geq 1.4v_{\text{beam}}/c$. Hence, for interplanetary bursts, $\Delta v_{\text{beam}}/v_{\text{beam}} \geq 0.3$ for the typical electron beam speed $v_{\text{beam}} = 0.2c$. However, observed electron beam widths²⁷ for interplanetary bursts extend well below this value, with $\Delta v_{\text{beam}}/v_{\text{beam}} = 0.1 - 0.4$. We conclude that the HOA is not applicable to the faster or narrower interplanetary type III beams. However, there is less constraint on the beam width for coronal bursts, and the HOA more accurately determines the rate in this case, provided the beams are not too fast. For both coronal and interplanetary type III bursts, the HOA underestimates the emission rate for the offset spectra believed present due to backscatter decay, in contrast to the result for symmetric primary and backscattered Langmuir spectra, where the HOA overestimates the emission rate.

The NSA is valid for when both $v_{\text{beam}} \leq c/\sqrt{3}$ and $\Delta v_{\text{beam}}/v_{\text{beam}} \leq 0.5$ are satisfied and hence is a good approximation for both coronal and interplanetary type III bursts. However, the relativistic beam speeds associated with the faster electron beams, in particular for the recently discovered type IIIId bursts,²⁸ have Langmuir wavenumbers $k_{\text{beam}} \leq k_T$, where coalescence between two Langmuir waves propagating in roughly the same direction is dominant. In this case neither approximation is valid, and the integral (24) must be evaluated numerically.

VI. CONCLUSION

In this paper, the second harmonic emission rate for the process $L(\omega_L(\mathbf{k}_1), \mathbf{k}_1) + L'(\omega_L(\mathbf{k}_2), \mathbf{k}_2) \rightarrow T(\omega_T(\mathbf{k}_T), \mathbf{k}_T)$ is considered for a Langmuir spectrum consisting of primary (forward propagating) and backward propagating (e.g., backscattered) Langmuir waves. Waves from the forward spectrum coalesce with waves from the backward spectrum to produce second harmonic waves at small wavenumbers. Two different types of Langmuir spectra are considered: Gaussian spectra which model the forward and backward spectra with Gaussian profiles, and arc spectra which also model the broader spread in perpendicular wavenumbers. The expres-

sion for the emission rate of second harmonic waves is reduced to a one-dimensional integral, which is evaluated numerically. An analytic expression for the emission rate is obtained after assuming the head-on approximation, often used to treat second harmonic emission. This approximation assumes the wavenumbers of the coalescing Langmuir waves far exceed that of the second harmonic waves, i.e., $k_L \gg k_T$, and is valid for spectral widths $K_L \gg |k_0 - k_T|$, where k_0 is the wavenumber offset in the Langmuir spectra. We introduce a more general narrow-spectrum approximation, which yields an improved analytic expression for the emission rate, valid to smaller k_L , assuming the Langmuir spectra are reasonably narrow; i.e., $K_L/k_L \leq 0.5$. Below, we summarize the results for the exact emission rate, and discuss the validity of the two approximations.

As a function of k_T and χ the exact emission rate for the Gaussian spectra peaks just above $k_{T0} = \sqrt{3}\omega_p/c$, and for $\chi \approx 45^\circ, 135^\circ$. For symmetric spectra ($k_b = -k_f$), the peaks at $\chi \approx 45^\circ$ and $\chi \approx 135^\circ$ are equal. For nonzero offsets ($k_0 > 0$), the emission rate is higher in the $\chi \approx 45^\circ$ peak. For arc spectra, the maxima occur at lower angles than for the Gaussian spectra, and the emission rate has a broader angular spread, due to the broader spread in perpendicular wavenumbers. At very low wavenumbers $k_f \leq k_T$, there is an additional effect due to two Langmuir waves able to coalesce while propagating in roughly the same direction. Hence, both coalescing waves come from the forward spectrum, or both come from the backward spectrum. In this case, the maximum emission rate occurs at $\chi = 0^\circ, 180^\circ$.

In the HOA, the emission rate always peaks at $\chi \approx 45^\circ, 135^\circ$, with symmetry about $\chi = 90^\circ$. Hence this approximation does not reproduce the above mentioned physical asymmetry associated with a wavenumber offset in the backward spectrum. The accuracy of the HOA in predicting the maximum emission rate depends on the offset k_0 . For $k_0 = 0$ (symmetric spectra), the HOA overestimates the maximum emission rate, particularly at small k_f . The HOA is most accurate for $k_0 \leq k_T$, where wavevector conservation is satisfied for the majority of Langmuir waves. For $k_0 > k_T$, the HOA underestimates the emission rate, particularly at low wavenumbers. Also, the HOA does not reproduce the peak in emission at small k_f , corresponding to coalescence between Langmuir waves propagating in roughly the same direction, because it assumes the coalescing Langmuir waves propagate in opposite directions. The accuracy of the HOA worsens with narrower Langmuir spectra, where it becomes more difficult to satisfy wavevector conservation while subject to $k_f \gg k_T$.

The NSA, on the other hand, successfully reproduces the higher emission rate in the $\chi \approx 45^\circ$ peak, associated with a wavenumber offset in the backscattered spectrum. The NSA

provides a good fit to the maximum emission rate, even at lower wavenumbers where the HOA breaks down. The accuracy of the NSA improves with narrower Langmuir spectra, and it works well for reasonably broad spectra ($K_f/k_f \leq 0.5$). However, the NSA also does not reproduce the peak in the emission rate at small wavenumbers, as coalescence between Langmuir waves propagating in the same direction cannot occur in the limit that the spectral width goes to zero.

The HOA works better for coronal type III bursts than for interplanetary type III bursts, a result of the dependence of the accuracy of the HOA on the wavenumber offset k_0 . The NSA works well in both cases. The applicability of these approximations to determining the degree of polarization of the resulting harmonic radiation is presently under investigation.

ACKNOWLEDGMENTS

The authors thank I. H. Cairns for helpful comments.

This work was supported by an Australian Postgraduate Award and the Australian Research Council.

- ¹D. F. Smith, *Adv. Astron. Astrophys.* **7**, 147 (1970).
- ²D. B. Melrose, *Space Sci. Rev.* **26**, 3 (1980).
- ³I. H. Cairns, Ph.D. thesis, University of Sydney, 1986.
- ⁴I. H. Cairns, *J. Plasma Phys.* **38**, 179 (1987).
- ⁵P. A. Robinson, A. J. Willes, and I. H. Cairns, *Astrophys. J.* **408**, 720 (1993).
- ⁶P. A. Robinson, D. L. Newman, and A. M. Rubenchik, *Phys. Fluids B* **4**, 2509 (1992).
- ⁷P. A. Robinson and D. L. Newman, *Phys. Fluids B* **1**, 2319 (1989).
- ⁸I. H. Cairns, *J. Plasma Phys.* **38**, 199 (1987).
- ⁹V. L. Ginzburg and V. V. Zheleznyakov, *Sov. Astron. J.* **2**, 653 (1958).
- ¹⁰D. B. Melrose, *Aust. J. Phys.* **23**, 871 (1970).
- ¹¹D. B. Melrose, *Aust. J. Phys.* **23**, 885 (1970).
- ¹²G. J. Nelson and D. B. Melrose, in *Solar Radiophysics*, edited by D. J. McLean and N. R. Labrum (Cambridge University Press, Cambridge, 1985), Chap. 13.
- ¹³I. H. Cairns, *J. Geophys. Res.* **95**, 3958 (1988).
- ¹⁴I. H. Cairns and D. B. Melrose, *J. Geophys. Res.* **90**, 6637 (1985).
- ¹⁵D. L. Newman, Ph.D. thesis, University of Colorado, 1985.
- ¹⁶P. H. Yoon, *Phys. Plasmas* **2**, 537 (1995).
- ¹⁷R. J.-M. Grogard, *Solar Phys.* **81**, 173 (1982).
- ¹⁸P. A. Sturrock, in *Physics of Solar Flares*, edited by W. H. Ness (National Aeronautics and Space Administration, Washington, DC, 1964), Sp-50.
- ¹⁹P. A. Robinson, I. H. Cairns, and D. A. Gurnett, *Astrophys. J.* **407**, 790 (1993).
- ²⁰P. A. Robinson and I. H. Cairns, *Astrophys. J.* **418**, 506 (1993).
- ²¹D. B. Melrose and J. E. Stenhouse, *Astron. Astrophys.* **73**, 151 (1979).
- ²²D. B. Melrose, G. A. Dulk, and D. E. Gary, *Proc. Astron. Soc. Aust.* **4**, 50 (1980).
- ²³C. Mercier, *Astron. Astrophys.* **130**, 119 (1990).
- ²⁴M. Abramowitz and I. A. Stegun, *Handbook of Mathematical Functions* (Dover, New York, 1972), p. 376.
- ²⁵G. A. Dulk, J. L. Steinberg, S. Hoang, and M. V. Goldman, *Astron. Astrophys.* **173**, 366 (1987).
- ²⁶S. Hoang, G. A. Dulk, and Y. Leblanc, *Astron. Astrophys.* **289**, 957 (1994).
- ²⁷R. P. Lin, D. W. Potter, D. A. Gurnett, and F. L. Scarf, *Astrophys. J.* **251**, 364 (1981).
- ²⁸M. Poquérusse, *Astron. Astrophys.* **286**, 611 (1994).